Kinetic Analysis of CO_2 Hydrogenation to Long-Chain Hydrocarbons on a Supported Iron Catalyst

Lucas Brübach,* Daniel Hodonj, and Peter Pfeifer

ABSTRACT: Hydrogenation of CO_2 to long chain hydrocarbons via combined reverse water gas shift (RWGS) and Fischer–Tropsch (FT) gained much attention in the last years as a way to produce sustainable hydrocarbons for the chemical industry or fuel applications. Despite the large amount of interest in the reaction, so far only a few studies have been conducted regarding the kinetics. In this study we carefully investigated the kinetics of an alumina supported iron catalyst at 280–320 °C, 10–20 bar, 900–120 000 $mL_N\,h^{-1}\,g^{-1}$, and a H_2/CO_2 molar inlet ratio of 2–4. Special attention was focused toward the thermodynamic constraints under reaction conditions. Based on elementary reaction steps according to recent mechanistic investigations, we derived new Langmuir–Hinshelwood–Hougen–Watson type kinetic expressions which allow an excellent reproduction of the experimental data and outperform existent models. Possible model combinations were discriminated against each other, and the best fit was obtained for the assumption of H assisted CO_2 and H assisted CO dissociation mechanisms for RWGS and FT, respectively. Model uncertainties that are introduced by the RWGS being close to equilibrium are discussed in detail and are possibly a reason for strongly varying results for activation energies between different studies. The detrimental effect of water vapor on the reaction progression is analyzed numerically and can be attributed to two parameters: kinetic inhibition via strong adsorption of oxygen containing species and thermodynamic constraints by shifting the equilibrium CO partial pressures to lower values.

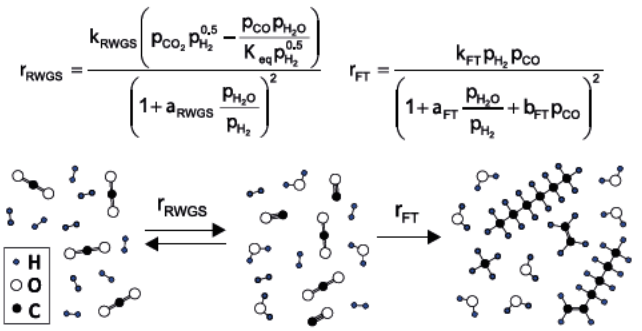

INTRODUCTION

Hydrocarbons derived from fossil resources are an indispen sable part of today's energy sector and chemical industry. However, the dramatic rise in greenhouse gas emissions and the associated risks of climate change call for a paradigm shift toward CO_2 neutral technologies.[1] While large parts of the energy sector can be electrified, certain fuels and chemicals will continue to require a hydrocarbon based feedstock.[2] Especially the aviation industry will continue using liquid hydrocarbon based fuels in the near future.[3,4] Therefore, there is a high need for sustainable processes for the production of hydrocarbons in the future. Catalytic hydrogenation of CO_2, derived from air or biomass, to long chain hydrocarbons offers a sustainable solution to this problem.

The reaction is usually reported to proceed via a two step mechanism.[5] CO_2 is first reduced to CO via the reverse water gas shift (RWGS) reaction (eq 1), and CO is then converted to a broad distribution of hydrocarbons via the Fischer–Tropsch (FT) reaction (eq 2; [1]calculated on the basis of *n* butane). Iron based catalysts are usually applied for the reaction since they catalyze both, the RWGS and FT reaction.[5] The direct conversion of CO_2 to hydrocarbons (direct hydrogenation, DH) can also be considered (eq 3; [1]calculated on the basis of *n* butane). Its contribution is usually reported to be relatively small, though.[6]

$$CO_2 + H_2 \rightleftharpoons CO + H_2O \quad \Delta H_R^0 = 41\ \mathrm{kJ\,mol^{-1}} \tag{1}$$

$$CO + 2H_2 \rightarrow (CH_2)^1 + H_2O \quad \Delta H_R^0 = -163\ \mathrm{kJ\,mol^{-1}} \tag{2}$$

$$CO_2 + 3H_2 \rightarrow (CH_2)^1 + 2H_2O \quad \Delta H_R^0 = -122\ \mathrm{kJ\,mol^{-1}} \tag{3}$$

The topic has attracted much attention in the past two decades. However, it has already been demonstrated during early Fischer–Tropsch research in Germany by Küster[7] that CO_2 can be hydrogenated to long chain hydrocarbons. Up to the mid 1990s there has only been a very limited number of publications from academia and industry aiming at the production of long chain hydrocarbons from CO_2.[8−10] Current research mainly focuses on catalyst development and is well summarized in several recent reviews.[5,11,12]

The kinetic modeling of the reaction has been addressed by only a few studies so far and is usually based on empirical Langmuir−Hinshelwood−Hougen−Watson (LHHW) type kinetic expressions. Riedel et al.[6] were the first to study the kinetics on a precipitated iron catalyst. They proposed three empirical LHHW type kinetic expressions accounting for the RWGS, FT, and DH reactions. Willauer et al.[13] omitted the kinetic expression for the DH reaction and adapted the model and most of the parameters to simulate their experimental data of an alumina supported iron based catalyst. Iglesias et al.[14] adapted the model without the DH reaction, as well, but refitted the parameters for their precipitated iron catalyst. Very recently, also Panzone et al.[15] adopted the Riedel model and extended it with an empirical chain growth probability model to describe the activity and product distribution of an alumina supported iron catalyst.

Meiri et al.[16] developed empirical LHHW type expressions that account for RWGS, FT, and oligomerization of 1 alkenes based on experimental investigations of an iron based spinel catalyst. The revised version of the model[17] was extended by alkene hydrogenation and consists of 20 reactions with 46 parameters. CO_2, CO, H_2, H_2O, *n* alkanes, and 1 alkenes up to C_5, oxygenates (lumped as butanoic acid), and long chain hydrocarbons (lumped as 1 decene) are considered.

Pour et al.[18,19] developed LHHW type kinetic models and fitted the parameters to experimental data from a precipitated iron catalyst investigated in a spinning basket reactor. A significant difference to previous modeling approaches is that their models are derived from elementary reaction steps and describe the consecutive reaction scheme with only one kinetic expression. However, such a model is only applicable for the case of complete backmixing and the RWGS being at its equilibrium. Owen et al.[20] analyzed the kinetics for the CO_2 hydrogenation over an iron silica catalyst and reported the apparent activation energies for methane formation and CO_2 consumption. Saeidi et al.[21] reviewed the mechanism and kinetics of CO_2 hydrogenation to value added products in detail. They put a special focus on how the model of Riedel et al.[6] can be derived from elementary reaction steps and derived new kinetic rate equations based on their proposed mechanism. However, they did not assess their model with experimental data.

Reviewing the existing work revealed that there has not been significant progress in the macrokinetic modeling of the reaction beyond empirical approaches. It is important to note, though, that there has been much progress in recent years in the mechanistic modeling and understanding of the reaction via density functional theory (DFT) calculations. Nie et al.[22,23] performed DFT calculations for Fe−Cu bimetallic catalysts to elucidate the reaction pathway depending on the catalyst composition, Hwang et al.[24] analyzed the promoting effect of Cu and K addition, and Han et al.[25] analyzed the active Fe phases for the CO_2 dissociation step. The studies agree in the fact that CO_2 dissociation is likely to proceed via a direct pathway or H assisted through a formate species while CO dissociation likely proceeds H assisted.

Based on these results we derived new LHHW type kinetic expressions that were assessed with carefully executed experiments and a thorough statistical analysis. For the experiments we applied a potassium doped alumina supported iron based catalyst (Fe/K@γ Al_2O_3).

EXPERIMENTAL SECTION

Catalyst Preparation. The alumina supported iron catalyst (Fe/K@γ Al_2O_3) was prepared with a two step incipient wetness impregnation method, adapted from Choi et al.[26] and Satthawong et al.[27] The support was impregnated with aqueous solutions of $Fe(NO_3)_3{\cdot}9H_2O$ (Supelco Emsure) and K_2CO_3 (Alfa Aesar) aiming at a nominal metal loading of 15 and 5.25 wt % (on support weight basis) of Fe and K, respectively.

The procedure was the following: 1.5 mm γ Al_2O_3 extrudates (Sasol Puralox TH 100) were crushed and sieved to the desired particle fraction of 100−200 μm. The support was then dried in an electric oven at 120 °C for 3 h under flowing air and impregnated with 0.9 mL $Fe(NO_3)_3$ solution per gram support. The impregnated powder was slightly stirred for 10 min and then dried again at 120 °C for 3 h under flowing air. The catalyst was calcined at 500 °C in a muffle furnace for 12 h (heating ramp: 1 K min^{-1}). The procedure was repeated for the K_2CO_3 impregnation. Finally, the agglomerates that were formed during the preparation were gently crushed and sieved again to obtain the desired particle fraction of 100−200 μm.

The BET surface area was determined to be 113 $m^2\,g^{-1}$. Pore volume and average pore diameter was measured via mercury porosimetry and determined to be 0.54 mL g^{-1} and 14 nm, respectively. Due to the high K_2CO_3 loading the catalyst is hygroscopic. Moisture absorption showed to have a detrimental effect on the catalyst stability and caused severe reproducibility issues of the experimental data several weeks after the catalyst preparation. The experimental data for the kinetic analysis shown here was obtained with one catalyst batch that was stored in a desiccator with silica gel for the whole time.

Experimental Setup. The experiments were carried out in a continuously operated lab scale setup with a tubular reactor as depicted in Figure 1. Gas flow rates of H_2 (>99.999%), CO_2 (>99.995%), CO (>99.8%), N_2 (>99.999%), and Ar

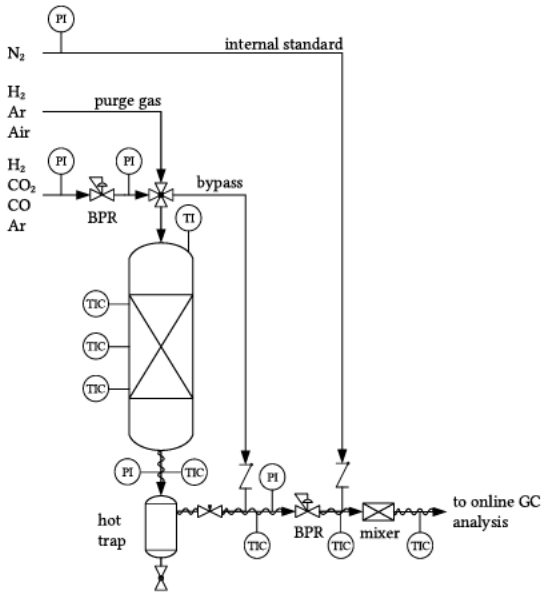

Figure 1. Simplified flow scheme of the lab scale setup (PI: pressure indicator, TI: temperature indicator, TIC: temperature indicator controller, BPR: back pressure regulator).

(>99.999%, all gases from Air Liquide) were controlled with mass flow controllers (Brooks SLA5850). Up and downstream pressures were regulated to guarantee calibration conditions of the devices at all time. The reactor consisted of a 1/2" stainless steel (1.4435) tube (ID: 8.5 mm) with three separately controlled aluminum heating jackets, each being 95 mm long with 5 mm distance from each other. The middle zone acted as the reaction zone whereas the lower and upper zone acted as buffer zones and were filled with inert silicon carbide particles (200−300 μm). Up to 2 g of catalyst (100−200 μm) were placed in the reaction zone and were diluted with an adequate amount of silicon carbide particles (200−300 μm) to the extent of the whole zone. The temperature along the reactor was measured with an axially movable thermocouple (type K) inserted into a centrally positioned 1/8" tube. The reactor effluent was led into a hot trap where long chain hydrocarbons (referred to as *wax phase*) and part of the water were condensed at 80 °C. The remaining gas was superheated and after the back pressure regulator (Equilibar LF Research Series) mixed with N_2 (internal standard for online GC analysis). The system pressure was monitored at several positions in the setup using electronic pressure transmitters (WIKA S 20). The relatively low temperature in the hot trap was necessary to avoid carry over issues of long chain hydrocarbons in the online GC.

Experimental Procedure. For the experiments, the reactor was filled with catalyst/diluent, integrated into the setup, pressurized with hydrogen to 10 bar above the later operating pressure, and checked for leakages with a H_2 semiconductor sensor. Prior to the startup of the reactor, the feed gas composition was checked via the bypass line. The deviation between the target flow rates and bypass measure ments was below 2% for all conditions.

For the catalyst activation a combined procedure consisting of reduction with hydrogen and subsequent carburization with diluted syngas was adapted from Landau et al.[28] The catalyst was first reduced with 100 $mL_N\ g_{Catalyst}^{-1}$ hydrogen at 450 °C (ramp: 1 K min^{-1}) for 16 h under atmospheric pressure. The reactor was then cooled down to 300 °C, and the catalyst was carburized with 200 $mL_N\ g_{Catalyst}^{-1}$ diluted syngas (molar ratio H_2/CO/Ar: 1/1/2) for 5 h. The setup was then pressurized with hydrogen, and the feed flow rates were set.

The investigated experimental conditions are summarized in Table 1. In total, 38 different conditions were studied. For each condition the reaction was maintained for at least 24 h to guarantee steady state conditions and produce a sufficient amount of wax for analysis. The temperature deviation within the catalyst bed was below ±2 K for all conditions (±1 K for most conditions). The startup condition was repeated after 3 days to check for catalyst deactivation. The catalyst was not operated for more than 150 h in one experimental series. An increased deactivation rate was observed at 320 °C for X_{CO_2} > 40%. We thus excluded the measurement with the highest residence time at 320 °C from the kinetic analysis.

Table 1. Experimental Conditions Investigated in This Study

T/°C	$(H_2/CO_2)_{in}$	p/bar	$GHSV$/$mL_N\ h^{-1}\ g^{-1}$	No. of conditions
280	3	10	900 120 000	8
300	2	10	900 7200	4
300	3	10	900 120 000	8
300	3	15	1800 14 400	4
300	3	20	3600 28 800	3
300	4	10	900 7200	4
320	3	10	900 120 000	7

Product Analysis. The online GC analysis was performed with a customized Agilent 8890 GC system (Teckso GmbH) employing 5 valves, 5 columns, and 3 detectors. H_2, CO_2, CO, N_2, and CH_4 were separated on two HaysepQ and an MS5A column and measured with a thermal conductivity detector (TCD). Short chain hydrocarbons (C_1−C_6) were separated on a GS GasPro column and detected with a flame ionization detector (FID). Long chain hydrocarbons up to C_{17} were separated on a HP 5 column and detected with an FID, as well. It has to be noted that short chain oxygenates up to C_3 which are formed in significant amounts during the reaction (especially ethanol) cannot be measured by the online GC.

H_2, CO_2, CO, and CH_4 were quantified with the internal standard N_2 via individual calibration curves that were determined with reference gas mixtures (basi Schöberl). The quantification of hydrocarbons was achieved using CH_4 as the reference gas with the assumption of a constant carbon number dependence relative to CH_4 for all components. The carbon balance of the gas phase analysis only was thereby closed between 89.9% to 99.8%.

The wax phase (C_7−C_{50}) that was drained from the hot trap was dissolved in *n* hexane (5 g L^{-1}, Supelco Suprasolv) and analyzed with a dedicated high temperature GC FID system (Agilent 7890B equipped with high temperature FID). The sample was introduced via direct injection with a program mable temperature inlet (Da Vinci Laboratory Solutions) to avoid discrimination of high boiling components. The separation was performed with an MXT 1 column (Restek, 30 m, 0.53 mm ID, 0.25 μm film). The analysis was done with a 100% method and response factors of 1 for all components.

The hydrocarbon product of the reaction is very complex with several hundred different species and can hardly be reliably resolved with our available 1 D GC FID analysis. Thus, we only allocated *n* alkanes and 1 alkenes up to C_{20}. All other species were lumped into the group *other* which includes iso alkanes, iso alkenes, linear alkenes with internal double bond, cyclo alkanes, aromatic components, and oxygenates.

The amount of wax that was drained from the hot trap was too small to be reliably quantified (neither by volume nor by weight if any was formed at all). From the analysis of short chain oxygenates from a representative water sample, we concluded that ∼80% of the deficit of the carbon balance belongs to the wax phase. Solid carbon formation was neglected. Based on pressure drop measurements, we did not find any evidence for excessive carbon formation during the reaction.

Data Analysis and Definitions. The residence time is given as either the gas hourly space velocity ($GHSV$) at normal conditions (0 °C and 1 atm) or as the modified residence time τ_{mod} under reaction conditions. Hereby, $\dot{V}_{in}$ denotes the volumetric flow rate at the reactor inlet under reaction conditions. Normal conditions are explicitly tagged with the subscript N. m_{cat} denotes the mass of the catalyst used.

$$GHSV = \frac{\dot{V}_{in,N}}{m_{cat}} \tag{4}$$

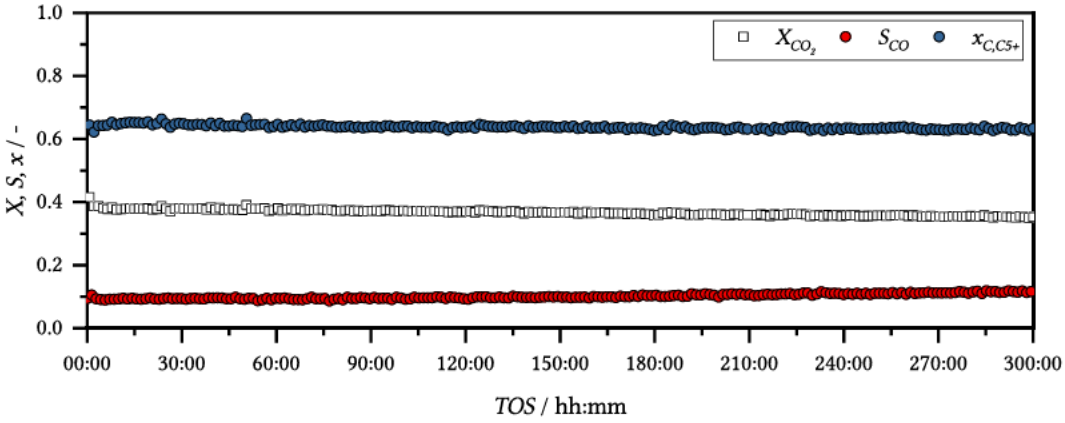

Figure 2. Development of CO_2 conversion (X_{CO_2}), CO selectivity (S_{CO}), and carbon based mole fraction of C_{5+} ($x_{C,C5+}$) over time on stream (TOS); Conditions: T = 300 °C, p = 10 bar, $(H_2/CO_2)_{in}$ = 3, $GHSV$ = 1800 $mL_N\,h^{-1}\,g^{-1}$, catalyst: Fe/K@γ Al_2O_3.

$$\tau_{mod} = \frac{m_{cat}}{\dot{V}_{in}} \tag{5}$$

The conversion X of CO_2 and H_2 was calculated from the molar flow rates at the inlet $\dot{n}_{i,in}$ and outlet $\dot{n}_{i,out}$ of the reactor.

$$X_i = \frac{\dot{n}_{i,in} - \dot{n}_{i,out}}{\dot{n}_{i,in}} \tag{6}$$

Product selectivities S_i were calculated on a carbon basis from the molar flow rates of species i divided by its carbon number $n_{c,i}$ with respect to the converted amount of CO_2.

$$S_i = \frac{\dot{n}_{i,out}}{n_{c,i}(\dot{n}_{CO_2,in} - \dot{n}_{CO_2,out})} \tag{7}$$

MODELING

Reactor Modeling. The investigated lab scale reactor was modeled as an isothermal, pseudohomogeneous, and isobaric ideal plug flow reactor (PFR). Axial dispersion ($L/d_P > 100$, $Bo > 50$) and wall effects ($d_R/d_P > 10$) could be considered negligible under the conditions applied. External mass transfer limitation as well as external and intraparticle heat transfer limitations of the catalyst particles could be neglected based on the criteria of Mears.[29] Intraparticle mass transfer limitation was negligible at the reactor inlet based on the criterion of Weisz and Prater.[30]

The steady state material balance for each component is given by eq 8. $\dot{n}_i$ is the molar flow rate of component i, m_{cat} is the catalyst mass, $\nu_{i,j}$ is the stoichiometric coefficient of component i in reaction j, and r_j is the rate of reaction j per mass of catalyst.

$$\frac{d\dot{n}_i}{dm_{cat}} = \sum_j \nu_{i,j} r_j \tag{8}$$

Kinetic Modeling. We propose new LHHW type kinetic rate expressions for the RWGS and FT reaction (eqs 9 and 10) which were derived from elementary reaction steps according to recent mechanistic studies.[22−25] The equations are based on the H assisted CO_2 and H assisted CO dissociation mecha nisms. Details about the model derivation and discrimination are given in the Supporting Information. A kinetic expression for the direct hydrogenation reaction (eq 3) was neglected, as it has already been proven valid by several authors before.[13,14,16] For the FT reaction, it was necessary to assume a representative pseudoproduct to correctly account for the changes in partial pressures during the reaction. We used a C_4 species which represented the average carbon number based on the molar product distribution of our experimental data. The temperature dependency of the rate constants k_i is given by a reparameterized Arrhenius equation (eq 11). The equilibrium constant K_{eq} of the RWGS reaction is given by an Antoine like equation (eq 12) for the temperature range 500−700 K. K_{eq} values were calculated from tabulated standard Gibbs energies of formation[31] and fitted to the given expression.

$$r_{RWGS} = \frac{k_{RWGS}\left(p_{CO_2}p_{H_2}^{0.5} - \frac{p_{CO}p_{H_2O}}{K_{eq}p_{H_2}^{0.5}}\right)}{\left(1 + a_{RWGS}\frac{p_{H_2O}}{p_{H_2}}\right)^2} \tag{9}$$

$$r_{FT} = \frac{k_{FT}p_{H_2}p_{CO}}{\left(1 + a_{FT}\frac{p_{H_2O}}{p_{H_2}} + b_{FT}p_{CO}\right)^2} \tag{10}$$

$$k_i = k_{i,ref}\exp\left(-\frac{E_{A,i}}{R}\left(\frac{1}{T} - \frac{1}{T_{ref}}\right)\right) \tag{11}$$

$$\log K_{eq} = 3.933 - \frac{4076}{T/K - 39.64} \tag{12}$$

Parameter Regression and Statistical Analysis. The parameters of the investigated kinetic model were regressed with a weighted least squares approach. The objective function was minimized with a global optimization method (*Global Search* in MATLAB) to achieve a high confidence that the optimal parameter estimates are actually found. In most cases, however, *GlobalSearch* converged directly to the global optimum within the first local solver (*fmincon*) call. The objective function of the algorithm was the sum of squares of the weighted residuals of the molar flow rates of CO_2 and CO (eq 13). Weighting with an estimate of the variance of the experimental values was necessary because the orders of magnitude of the numbers varied significantly. Strictly, reliable estimates of the variance for every experimental conditions would be only accessible via reproduction of every condition.

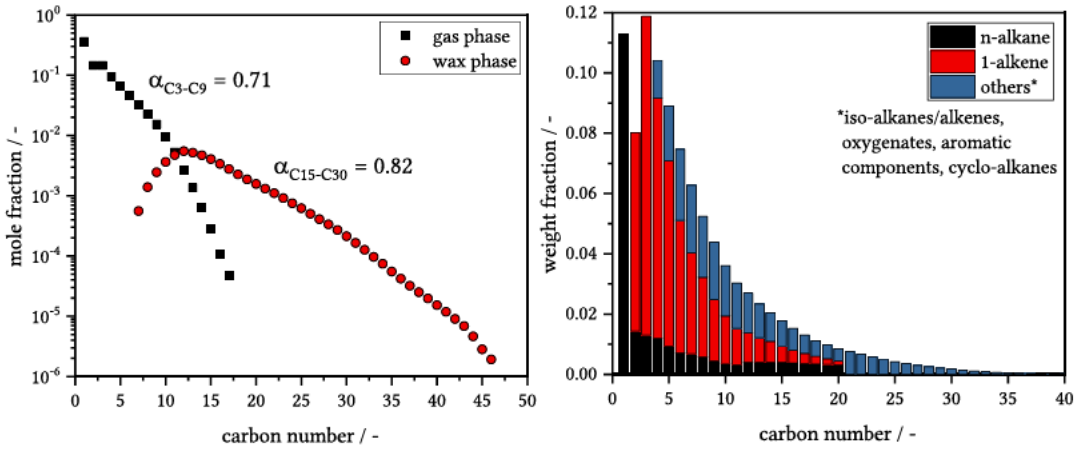

Figure 3. Hydrocarbon product distribution as an ASF plot (left) and mass distribution (right). Conditions: T = 300 °C, p = 10 bar, $(H_2/CO_2)_{in}$ = 3, $GHSV$ = 900 $mL_N\,h^{-1}\,g^{-1}$, X_{CO2} = 41%, catalyst: Fe/K@γ Al_2O_3.

Table 2. Performance of Selected Catalysts with a High Selectivity to Long Chain Hydrocarbons in Fixed Bed Reactors at T = 300 °C, p = 10 bar, $(H_2/CO_2)_{in}$ = 3 and Similar *GHSV*

				Hydrocarbon distribution[a]		
Catalyst	$GHSV$/mL h^{-1} g^{-1}	X_{CO_2}/%	S_{CO}/%	CH_4/%	C_2 C_4/%	C_{5+}/%
Fe/K@γ-Al_2O_3 (this study, 100 h *TOS*)	1800	37	10	10	27	63
Fe/K@γ-Al_2O_3[34]	1800	31	22	11	36	53
Fe-Cu-Al-K[35]	2000	36	10	11	35	54
Fe/La/Cu/K@TiO_2[36]	1320	27	32	10	31	59
$CuFeO_2$-6[37]	1800	17	32	3	31	66

[a]Hydrocarbon distribution is given as a carbon based mole fraction (excluding CO).

However, this would have meant months of additional experimental work. We thus estimated a constant relative error from experiments at our reference condition (T = 300 °C, p = 10 bar, $(H_2/CO_2)_{in}$ = 3, $GHSV$ = 1800 $mL_N\,h^{-1}\,g^{-1}$). The uncertainty of the molar flow rate of CO was approximately 3 times larger than for CO_2. The simulated flow rates $\dot{n}_{i,sim}$ were calculated by solving the material balance (eq 8) with the ordinary differential equation solver *ode15s* in MATLAB for each experimental condition j.

$$F = \sum_j \sum_i \frac{(\dot{n}_{i,\mathrm{sim}} - \dot{n}_{i,\mathrm{exp}})^2}{s_i^2} \tag{13}$$

For the statistical analysis, the Jacobian matrix was numerically approximated at the global solution and used to calculate the approximate correlation matrix and individual linearized 95% confidence intervals of the parameters. For the assessment of the adequacy of the linearly approximated confidence intervals, we evaluated the profile t function as suggested by Bates and Watts.[32]

RESULTS AND DISCUSSION

Experimental Results. *Catalyst Stability.* The long term stability of the catalyst was investigated over 300 h time on stream (*TOS*) under typical reaction conditions as shown in Figure 2. The selectivity to hydrocarbons with 5 and more carbon atoms is given as a carbon based mole fraction (excluding CO). Catalyst activity and selectivity stabilized rapidly after the startup of the reaction within a few hours. Afterward the catalyst went into a pseudosteady state with a slow and constant deactivation. The CO_2 conversion decreased while the CO selectivity increased. The product distribution within the hydrocarbons remained constant, though. Based on these results we conducted our kinetic study between 24 and 150 h *TOS* for each catalyst loading to avoid a bias of the data via catalyst deactivation. The pressure drop over the reactor remained constant for the whole experiment.

Similar to the findings of Iglesias et al.[14] we observed a threshold CO_2 conversion above which the catalyst rapidly deactivated. For our catalyst, X_{CO_2} > 40% could not be maintained steadily at $(H_2/CO_2)_{in}$ = 3.

Catalyst Performance. A typical product distribution of the investigated Fe/K@γ Al_2O_3 catalyst is shown in Figure 3 as a logarithmic mole fraction (so called Anderson–Schulz–Flory plot) and as a weight fraction. From the Anderson–Schulz–Flory (ASF) plot, one can obtain the chain growth probability α via linear regression analysis. The product displays a 2 α distribution with an α value of ~0.7 for the short chain products and ~0.8 for the long chain products. A 2 α distribution is often observed in conventional low temperature Fischer–Tropsch processes with cobalt and iron catalysts.[33] This effect is usually explained with secondary chain formation reactions of 1 alkenes in the liquid phase in the catalyst pores. Therefore, the primary selectivity to long chain hydrocarbons needs to be sufficiently high.[33]

The hydrocarbons mainly consist of short chain 1 alkenes up to C_{10} as it can be seen in Figure 3. The share of 1 alkenes within one carbon number decreases significantly with increasing chain length while the share of *others* and *n* alkanes increases. Oxygenates up to C_3 are not measured in our experimental setup (see section 2). Especially the C_2 fraction would be significantly higher when oxygenates could be considered.

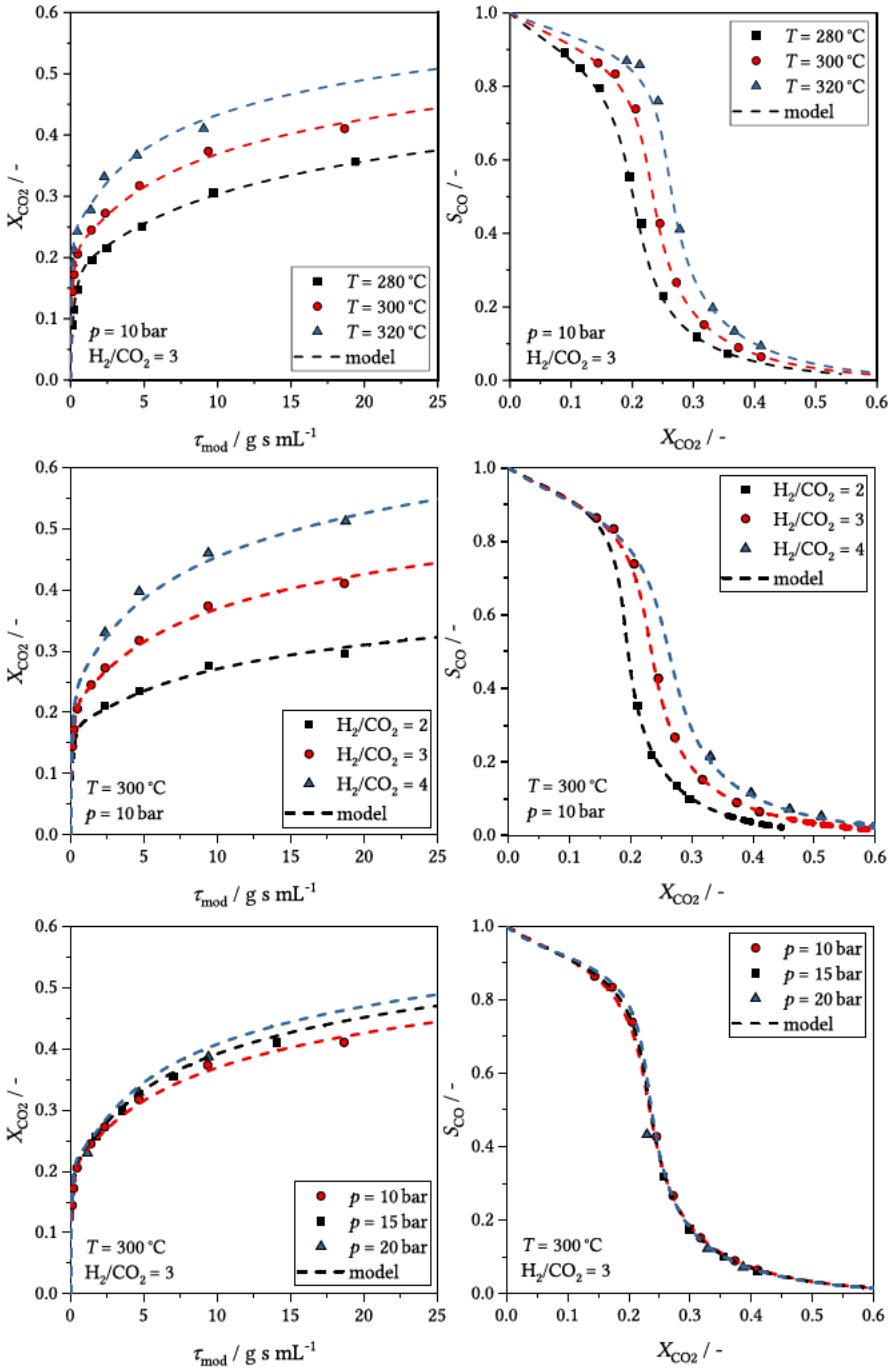

Figure 4. CO_2 conversion versus modified residence time (left) and CO selectivity versus CO_2 conversion (right) for different temperatures (first row), H_2/CO_2 inlet ratios (second row) and pressures (third row). Data points correspond to experimental values and dashed lines to simulation results. Conditions: T = 280−320 °C, p = 10−20 bar, $(H_2/CO_2)_{in}$ = 2−4, *GHSV* = 900−120 000 $mL_N\,h^{-1}\,g^{-1}$, catalyst: Fe/K@γ Al_2O_3.

The catalyst performance is consistent with previous studies of the catalyst system under similar conditions[34] as shown in Table 2. However, we observed a higher catalytic activity, which may be attributed to the slightly different preparation and the improved catalyst activation procedure. Several other catalyst systems with a high selectivity to long chain hydro carbons are given in Table 2. The comparison of the selectivity to long chain products between different studies is difficult because it is often not clear to which extent short chain oxygenates are considered. These species may be formed in large quantitites. However, despite the simple composition and preparation of the catalyst, it performs well with respect to activity and selectivity.

Parameter Study. The results of the catalytic activity measurements are given in Figure 4. The CO_2 conversion rises rapidly at low residence times with CO as the main product and starts to flatten at $X_{CO_2} \approx$ 20−25% (for $(H_2/CO_2)_{in}$ = 3). The consecutive character of the reaction is clearly visible from the course of the CO selectivity. At low CO_2 conversion levels, CO is the main product from the RWGS reaction which is then converted to hydrocarbons via the FT reaction. Increasing the temperature significantly accelerates the reaction rate and

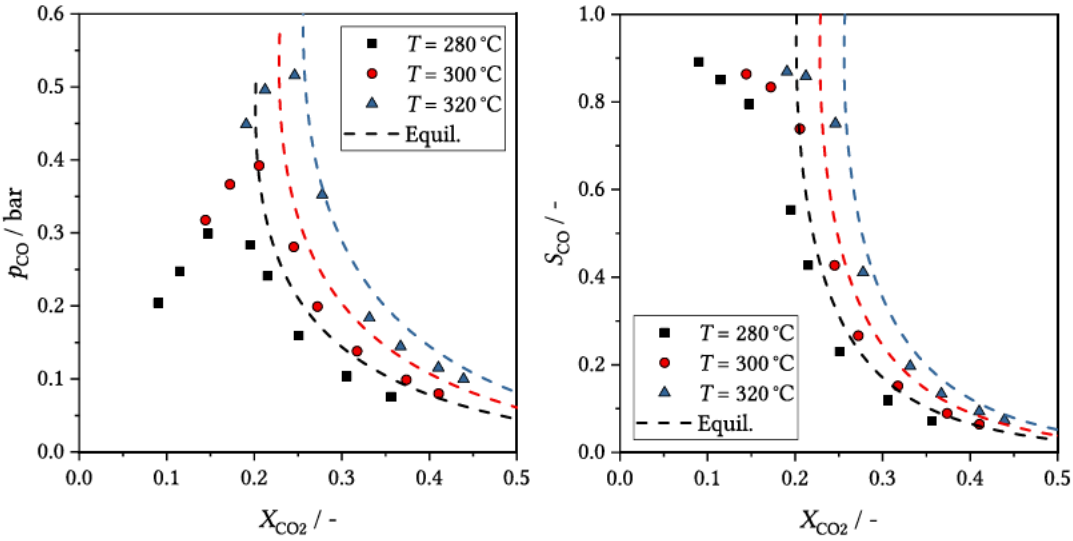

Figure 5. CO partial pessure versus CO_2 conversion (left) and CO selectivity versus CO_2 conversion (right): Data points correspond to experimental values and dashed lines to theoretical equilibrium calculations with the assumption of an ideal gas phase. Conditions: T = 280–320 °C, p = 10 bar, $(H_2/CO_2)_{in}$ = 3, *GHSV* = 900–120 000 $mL_N\,h^{-1}\,g^{-1}$, catalyst: Fe/K@γ Al_2O_3.

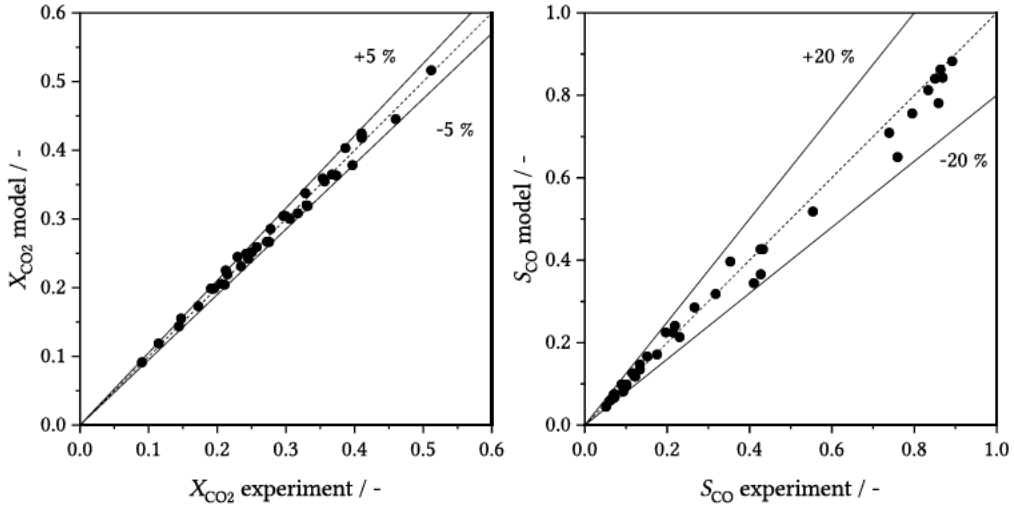

Figure 6. Parity plot for CO_2 conversion (left) and CO selectivity (right). Conditions: T = 280–320 °C, p = 10–20 bar, $(H_2/CO_2)_{in}$ = 2–4, *GHSV* = 900–120 000 $mL_N\,h^{-1}\,g^{-1}$, catalyst: Fe/K@γ Al_2O_3.

shifts the CO selectivity to higher values at the same CO_2 conversion. The same effect can be observed when increasing the H_2/CO_2 ratio. A pressure increase from 10 to 20 bar led to a significant increase of CO_2 conversion at the same absolute flow rates. However, this is mainly an effect of increased residence time. When plotting X_{CO_2} versus τ_{mod}, one can see that the conversion increases only slightly upon increasing the pressure. This means that the overall apparent reaction order is slightly greater than 1. Kinetic experiments at a lower pressure (5 bar) failed due to increased catalyst deactivation.

The characteristic course of CO_2 conversion, CO selectivity, and the influence of thermodynamic equilibrium has been discussed contradictory in the literature.[5] Undoubtedly, the RWGS reaction alone is thermodynamically limited at 300 °C with an equilibrium CO_2 conversion of ~23 %. Due to the continuous removal of CO by the FT reaction, higher CO_2 conversions are possible. However, the increasing partial pressure of H_2O in the gas mixture by both RWGS and FT reduces the maximum possible CO partial pressure at equilibrium with increasing CO_2 conversion. Assuming a continuous removal of excess CO by FT according to eqs 1 and 2 with the RWGS reaction being at the thermodynamic equilibrium one can calculate the maximum possible CO partial pressure in the gas mixture. This is illustrated in Figure 5 in comparison to the experimental data for CO partial pressure and CO selectivity. The RWGS reaction is close to equilibrium, and the CO selectivity follows the trend imposed by the thermodynamic constraint at X_{CO_2} > 20–25%. The overall CO_2 consumption rate is thus controlled by the FT reaction at X_{CO_2} > 20–25%. Some authors exhibited the same behavior for other iron based catalyst systems: A fast RWGS that (almost) reaches equilibrium followed by a slow FT reaction being the rate determining step.[6,13,36] Iglesias et al.[14] reported the opposite.

The decreasing CO partial pressure imposed by the thermodynamic equilibrium of the RWGS reaction is one of the main reasons for the stagnation of CO_2 conversion at increased residence times. Additionally, kinetic inhibition by

Table 3. Estimated Parameters of the Proposed Kinetic Model with Individual Linearized 95% Confidence Intervals and Approximate Correlation Matrix

			95% confidence interval								
Parameter	Unit	Estimated value	absolute	relative	Approximate correlation matrix						
$k_{RWGS,300\ °C}$	mol h^{-1} g^{-1} $bar^{-1.5}$	8.13×10^{-2}	$\pm 1.92 \times 10^{-2}$	±24%	1.00	0.39	0.54	0.38	**0.92**	0.45	0.34
$k_{FT,300\ °C}$	mol h^{-1} g^{-1} bar^{-2}	6.39×10^{-2}	$\pm 3.03 \times 10^{-2}$	±47%		1.00	0.04	0.38	0.26	**0.99**	**0.97**
$E_{A,RWGS}$	kJ mol^{-1}	1.15×10^{2}	$\pm 1.60 \times 10^{1}$	±14%			1.00	0.50	0.47	0.07	0.01
$E_{A,FT}$	kJ mol^{-1}	6.78×10^{1}	±8.51	±13%				1.00	0.33	0.40	0.37
a_{RWGS}		1.63×10^{1}	±3.54	±22%					1.00	0.32	0.24
a_{FT}		9.07	±2.86	±31%						1.00	**0.93**
b_{FT}	bar^{-1}	2.44	±1.01	±41%							1.00

H_2O is usually observed for iron based FT catalysts.[38] The individual contribution of the two effects will be analyzed with the developed kinetic model in the next section.

Kinetic Analysis. *Model Performance.* The comparison of model results with experimental data is shown in Figure 4. The parity plots of CO_2 conversion and CO selectivity are given in Figure 6. In general, a very good agreement of the experimental data with the model could be achieved. The calculated CO_2 conversions deviate less than 5% from the experimental values. The deviation may appear higher from Figure 4, though. One has to keep in mind that the model is solved individually for each experimental condition in the regression process taking into account small deviations of the feed flow rates. The calculated CO selectivities deviate less than 20% from the experimental values. The higher deviation is not surprising since the CO molar flow rates had a 3 fold higher measurement uncertainty and the selectivity is a derived measure from two quantities. The relationship between CO_2 conversion and CO selectivity, however, is correctly described by the model as shown in Figure 4. The maximum relative deviations of the molar flow rates of CO_2 and CO (which were actually fitted) were 3% and 10%, respectively.

The estimated parameters with their individual linearized 95% confidence regions and the approximate correlation matrix are given in Table 3. Each of the parameters is statistically significant with relative uncertainties ranging from 13% to 47%. Based on the evaluation of the profile t functions,[32] the linearly approximated confidence intervals are reasonable estimates of the inference regions except for $k_{FT,300\ °C}$. A precise 95% confidence interval of $k_{FT,300\ °C}$ is given by $[4.28 \times 10^{-2}, 1.07 \times 10^{-1}]$ as opposed to $[3.36 \times 10^{-2}, 9.42 \times 10^{-2}]$ in the linearized case.

The reaction rate constants are heavily correlated with the inhibition coefficients in the denominator which is an implicit problem of LHHW kinetic expressions due to the model structure. Ratkowsky[39] proposed a reparameterization for LHHW kinetic expressions which leads to statistically more well behaved parameter estimates. However, it does not allow for the simultaneous regression of reaction rate constants and activation energies which is similarly undesirable.

The high uncertainty of the FT parameters is caused by the consideration of CO inhibition in the denominator of the FT rate expression (see eq 10). Statistically more well behaved parameter estimates can be obtained when it is neglected. The overall model performance is worse in this case, though (see Supporting Information). The CO partial pressures are rather low under the observed conditions. Thus, the inhibiting influence on the kinetics is smaller than under traditional FT conditions and prone to a larger uncertainty. Nevertheless, as the inhibiting effect of CO is usually important for the kinetic modeling of iron based FT catalysts[40,41] and the overall fitting result was significantly improved, we kept it.

We also assessed the model of Riedel et al.[6] (which is widely used in the literature[13−15]) for our experimental data. The model can reproduce the data satisfactorily but strongly suffers from statistically ill behaved parameters (for details see Supporting Information). Riedel et al.[6] adapted existing rate expressions of FT and WGS for their model which were not developed for the special conditions of CO_2−FT. From this point of view, the poor performance is not surprising. Results for the model of Saeidi et al.[21] and additional model modifications which may be considered for our model are shown and discussed in the Supporting Information.

Influence of RWGS Equilibrium. It is usually good practice to measure the kinetic data of a reaction far from its equilibrium to avoid any bias of the parameter estimates. However, this could not be avoided here due to the different reaction rates of FT and RWGS. Figure 5 shows clearly that the RWGS was close to equilibrium for most of the investigated conditions. During the model discrimination we observed that the overall model performance was hardly affected by the assumed reaction pathway for the RWGS step. For our available data, it was most important to consider the equilibrium and kinetic inhibition by water (here via adsorbed oxygen species). More insights into the RWGS reaction could only be obtained with detailed experiments within the kinetic regime. For the FT reaction however, we could clearly obtain the best fit under the assumption of H assisted CO dissociation with the second hydrogenation step being rate determining (see Supporting Information). This has also been reported for the traditional FT synthesis.[42]

The bias introduced by the RWGS equilibrium may explain significantly varying results between different kinetic studies. Table 4 summarizes the reported activation energies. To some

Table 4. Reported Activation Energies of RWGS and FT for the Hydrogenation of CO_2 to Hydrocarbons for Different Catalysts (Relative Composition Is Given on Weight Basis)

	E_A/kJ mol^{-1}	
Catalyst	RWGS	FT
15Fe/5.25K@100γ-Al_2O_3 (This study)	115	68
15Fe/10K@100γ-Al_2O_3[15]	73	50
100Fe/13Al_2O_3/10Cu/10K[6]	55	72
100Fe/2K[14]	139	95
100Fe/10K[44]	119	71
100Fe-Al-O spinel/4K[16]	72	
100Fe/3K/2.6Cu[19]		~20[a]

[a]RWGS assumed to be in equilibrium.

extent, the catalyst composition determines the kinetic parameters (e.g., the influence of Cu promotion on the catalyst performance is highlighted in several studies, both experimentally and theoretically[22,23,25,36,43]). However, the RWGS being close to equilibrium seems to be a large problem during parameter estimation and may lead to surprising results like in the work of Pour and Housaindokht[19] who report an apparent activation energy for the FT reaction of ~20 kJ mol^{-1} (under the assumption of the RWGS reaction being in equilibrium). Usually, reported activation energies of the FT reaction on iron catalysts fall within the range 55−105 kJ mol^{-1}.[41]

Despite the many uncertainties, one is confronted with in this challenging reaction we think that it is still possible to derive reliable kinetic models which may be employed e.g. for the design of industrial reactors. However, one has to keep in mind that the parameters may be biased and do not necessarily represent chemically intrinsic values. From a mathematical point of view, though, this fact should be of minor concern.

Decomposition of FT Reaction Rate. A question that requires additional attention is whether the decreasing CO partial pressure imposed by the thermodynamic equilibrium or the kinetic inhibition is the main driver for the stagnation of CO_2 conversion at high residence times. This can be analyzed by splitting the kinetic expression of the FT reaction into two parts: the driving force of the reaction normalized with its maximum value (β, eq 14) and the inhibition factor (γ, eq 15).

$$\beta = \frac{p_{H_2} p_{CO}}{\max(p_{H_2} p_{CO})} \tag{14}$$

$$\gamma = \frac{1}{\left(1 + a_{FT}\frac{p_{H_2O}}{p_{H_2}} + b_{FT} p_{CO}\right)^2} \tag{15}$$

Figure 7 shows the result of a simulation at T = 300 °C, p = 10 bar and $(H_2/CO_2)_{in}$ = 3. At low CO_2 conversions, only small amounts of CO have already been formed by the RWGS reaction which leads to a low driving force for the FT reaction. β goes through a maximum at the maximum CO partial pressure and starts to decrease after that. The H_2 partial pressure decreases, as well. However, it has only a minor contribution. It decreases from 7.5 bar at the reactor entrance to ~5.5 bar at X_{CO_2} = 40%. With an increasing CO_2 conversion the inhibition factor γ decreases strongly and is well below β. For X_{CO_2} > 30%, γ is mainly determined by the water partial pressure. So, according to our model, the kinetic inhibition by water seems to be the main reason for the stagnation of CO_2 conversion at high residence times. This result highlights the importance of continuous water removal in technical realizations.

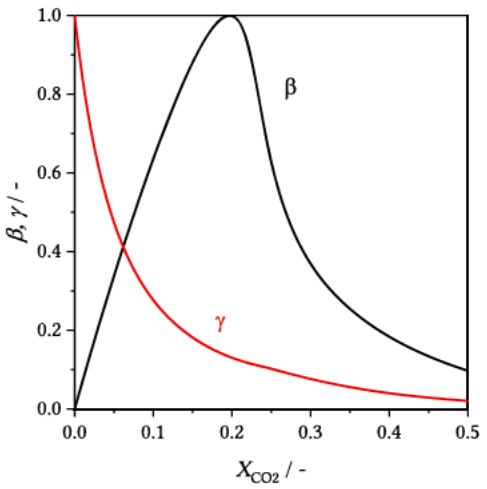

Figure 7. Numeric split of the FT reaction rate: β, relative kinetic driving force; γ, inhibition factor. Conditions: T = 300 °C, p = 10 bar, $(H_2/CO_2)_{in}$ = 3.

CONCLUSION AND OUTLOOK

The hydrogenation of CO_2 to olefin rich, long chain hydro carbons is a promising route for the production of sustainable hydrocarbons for fuels and chemicals in the future. The kinetics of the reaction are highly important for the design and techno economic assessment of chemical plants that might utilize this reaction and were thus carefully analyzed in this study.

Our analysis of an in house prepared Fe/K@γ Al_2O_3 catalyst revealed that the reaction can be well described with simple LHHW type kinetic expressions for RWGS and FT derived from elementary reaction steps. The best performing model was derived under the assumption of H assisted CO_2 and H assisted CO dissociation mechanisms which are supported by recent mechanistic studies. The statistical analysis revealed some uncertainty of the parameter estimates and a strong correlation of the inhibition coefficients and the reaction rate constants. Unfortunately, this seems to be unavoidable due to the mathematical structure of LHHW expressions. The reported activation energies for the RWGS and FT reaction in the literature differ significantly from each other (including our estimates). Additionally to the influence of the applied catalyst the thermodynamic limitation of the RWGS seems to introduce a strong bias to the kinetic parameter estimation. This may complicate the comparison of different studies but should not present a problem when applying the model for real reactor designs. The decomposition of the FT reaction rate into a driving force and an inhibition factor revealed that kinetic inhibition by water is the main reason for low reaction rates at high residence times according to our model.

Modeling of the product distribution has only been addressed by a simple chain growth probability factor in this study. It is highly desirable to model the catalytic activity and selectivity of the reaction consistently with only one model. Ideally, this model should also be able to account for secondary reactions of light products so that the effects of a recycle of light products and unconverted feed gas can be sufficiently well described. We are currently working on such a model and will assess the adequacy under realistic recycle conditions in follow up manuscripts.

ASSOCIATED CONTENT

Supporting Information

The Supporting Information is available free of charge at https://pubs.acs.org/doi/10.1021/acs.iecr.1c04018.

Details about kinetic model derivation and discrim ination (PDF)

AUTHOR INFORMATION

Corresponding Author

Lucas Brübach − *Institute for Micro Process Engineering, Karlsruhe Institute of Technology, 76 344 Eggenstein Leopoldshafen, Germany;* orcid.org/0000 0002 9530 8256; Phone: +49 (0)721 608 24 094; Email: lucas.bruebach@kit.edu

Authors

Daniel Hodonj − *Institute for Micro Process Engineering, Karlsruhe Institute of Technology, 76 344 Eggenstein Leopoldshafen, Germany*

Peter Pfeifer − *Institute for Micro Process Engineering, Karlsruhe Institute of Technology, 76 344 Eggenstein Leopoldshafen, Germany*

Notes

The authors declare no competing financial interest.

■ ACKNOWLEDGMENTS

This work was funded by the German Federal Ministry for Economic Affairs and Energy (BMWi) under the project acronym PowerFuel, Grant Number 03EIV071B. The authors thank Malina Burcea (Institute of Chemical Process Engineering KIT) and Dr. Peter Weidler (Institute of Functional Interfaces KIT) for support with the physical characterization of the catalyst.

SYMBOLS

α	chain growth probability
a_i	inhibition coefficient for H_2O in reaction i
b_i	inhibition coefficient for CO in reaction i (bar^{-1})
β	relative kinetic driving force
Bo	Bodenstein number
d_P	particle diameter (m)
d_R	reactor diameter (here: width of annulus between outer wall and central tube, m)
γ	inhibition factor
E_A	activation energy ($kJ\,mol^{-1}$)
F	objective value of minimization function (eq 13)
$GHSV$	gas hourly space velocity ($mL_N\,h^{-1}\,g^{-1}$)
ΔH_R^0	enthalpy of reaction at standard conditions (25 °C and 1 atm, $kJ\,mol^{-1}$)
K_{eq}	equilibrium constant of RWGS reaction
k_i	reaction rate constant of reaction i ($mol\,h^{-1}\,g^{-1}\,bar^{-2}$)
$k_{i,ref}$	reaction rate constant of reaction i at reference temperature ($mol\,h^{-1}\,g^{-1}\,bar^{-2}$)
L	catalyst bed length (m)
m	mass (kg)
$n_{c,i}$	number of carbon atoms in component i
$\dot{n}_i$	molar flow rate of component i ($mol\,h^{-1}$)
$\nu_{i,j}$	stoichiometric coefficient
p	pressure (bar)
p_i	partial pressure of component i (bar)
r_i	reaction rate of reaction i ($mol\,h^{-1}\,g^{-1}$)
s^2	estimate of variance
S_i	carbon based selectivity of component i
T	temperature (°C/K)
T_{ref}	reference temperature (here: 300 °C)
τ_{mod}	modified residence time ($g\,s\,cm^{-3}$)
V_N	volumetric flow rate at normal conditions (0 °C and 1 atm, $mL_N\,min^{-1}$)
$x_{C,CS+}$	carbon based mole fraction of hydrocarbons with 5 and more carbon atoms (excluding CO)
X_i	conversion of component i

SUBSCRIPTS AND SUPERSCRIPTS

cat	catalyst
exp	experimental value
i, j	species i/j
in	reactor inlet
N	normal conditions (0 °C and 1 atm)
out	reactor outlet
sim	simulated value

ABBREVIATIONS

ASF	Anderson−Schulz−Flory
BET	Brunauer−Emmet−Teller
BPR	back pressure regulator
DFT	density functional theory
DH	direct hydrogenation
Equil.	thermodynamic equilibrium
FID	flame ionization detector
FT	Fischer−Tropsch
FTS	Fischer−Tropsch synthesis
GC	gas chromatograph
LHHW	Lamgmuir−Hinshelwood−Hougen−Watson
PI	pressure indicator
RWGS	reverse water gas shift
TCD	thermal conductivity detector
TI	temperature indicator
TIC	temperature indicator controller
TOS	time on stream
WGS	water gas shift

REFERENCES

(1) Chu, S.; Majumdar, A. Opportunities and challenges for a sustainable energy future. *Nature* **2012**, *488*, 294−303.

(2) Graves, C.; Ebbesen, S. D.; Mogensen, M.; Lackner, K. S. Sustainable hydrocarbon fuels by recycling CO2 and H2O with renewable or nuclear energy. *Renewable Sustainable Energy Rev.* **2011**, *15*, 1−23.

(3) Holladay, J.; Abdullah, Z.; Heyne, J. *Sustainable Aviation Fuel: Review of Technical Pathways*: Report No. DOE/EE 2041; U.S. Department of Energy, Office of Energy Efficiency and Renewable Energy: Washington, DC, 2020.

(4) Bauen, A.; Bitossi, N.; German, L.; Harris, A.; Leow, K. Sustainable Aviation Fuels. *Johnson Matthey Technol. Rev.* **2020**, *64*, 263−278.

(5) Panzone, C.; Philippe, R.; Chappaz, A.; Fongarland, P.; Bengaouer, A. Power to Liquid catalytic CO2 valorization into fuels and chemicals: focus on the Fischer−Tropsch route. *J. CO2 Util.* **2020**, *38*, 314−347.

(6) Riedel, T.; Schaub, G.; Jun, K. W.; Lee, K. W. Kinetics of CO2 Hydrogenation on a K Promoted Fe Catalyst. *Ind. Eng. Chem. Res.* **2001**, *40*, 1355−1363.

(7) Küster, H. Über die Reduktion der Kohlensäure zu höheren Kohlenwasserstoffen bei Atmosphärendruck an Katalysatoren der Eisengruppe. *Brennst. Chem.* **1936**, *17*, 221−228.

(8) Russell, W. W.; Miller, G. H. Catalytic Hydrogenation of Carbon Dioxide to Higher Hydrocarbons. *J. Am. Chem. Soc.* **1950**, *72*, 2446−2454.

(9) Kölbel, H.; Ackermann, P. Process for catalytic reduction of carbon dioxide with hydrogen. U.S. Patent 2,692,274. 1954.

(10) Fiato, R. A.; Soled, S. L.; Rice, G. W.; Miseo, S. Method for producing olefins from H_2 and CO_2 using an iron carbide based catalyst. U.S. Patent 5,140,049A. 1992.
(11) Ra, E. C.; Kim, K. Y.; Kim, E. H.; Lee, H.; An, K.; Lee, J. S. Recycling Carbon Dioxide through Catalytic Hydrogenation: Recent Key Developments and Perspectives. *ACS Catal.* **2020**, *10*, 11318−11345.
(12) Gao, P.; Zhang, L.; Li, S.; Zhou, Z.; Sun, Y. Novel Heterogeneous Catalysts for CO2 Hydrogenation to Liquid Fuels. *ACS Cent. Sci.* **2020**, *6*, 1657−1670.
(13) Willauer, H. D.; Ananth, R.; Olsen, M. T.; Drab, D. M.; Hardy, D. R.; Williams, F. W. Modeling and kinetic analysis of CO2 hydrogenation using a Mn and K promoted Fe catalyst in a fixed bed reactor. *J. CO2 Util.* **2013**, *3*−*4*, 56−64.
(14) Iglesias, G. M.; de Vries, C.; Claeys, M.; Schaub, G. Chemical energy storage in gaseous hydrocarbons via iron Fischer−Tropsch synthesis from H_2/CO_2—Kinetics, selectivity and process consid erations. *Catal. Today* **2015**, *242*, 184−192.
(15) Panzone, C.; Philippe, R.; Nikitine, C.; Vanoye, L.; Bengaouer, A.; Chappaz, A.; Fongarland, P. Catalytic and Kinetic Study of the CO2 Hydrogenation Reaction over a Fe−K/Al2O3 Catalyst toward Liquid and Gaseous Hydrocarbon Production. *Ind. Eng. Chem. Res.* **2021**, *60*, 16635−16652.
(16) Meiri, N.; Dinburg, Y.; Amoyal, M.; Koukouliev, V.; Nehemya, R. V.; Landau, M. V.; Herskowitz, M. Novel process and catalytic materials for converting CO2 and H2 containing mixtures to liquid fuels and chemicals. *Faraday Discuss.* **2015**, *183*, 197−215.
(17) Meiri, N.; Radus, R.; Herskowitz, M. Simulation of novel process of CO2 conversion to liquid fuels. *J. CO2 Util.* **2017**, *17*, 284−289.
(18) Pour, A. N.; Housaindokht, M. R.; Monhemi, H. A new LHHW kinetic model for CO2 hydrogenation over an iron catalyst. *Prog. React. Kinet. Mech.* **2016**, *41*, 159−169.
(19) Pour, A. N.; Housaindokht, M. R. A new kinetic model for direct CO2 hydrogenation to higher hydrocarbons on a precipitated iron catalyst: Effect of catalyst particle size. *J. Energy Chem.* **2017**, *26*, 359−367.
(20) Owen, R. E.; Mattia, D.; Plucinski, P.; Jones, M. D. Kinetics of CO2 Hydrogenation to Hydrocarbons over Iron Silica Catalysts. *ChemPhysChem* **2017**, *18*, 3211−3218.
(21) Saeidi, S.; Najari, S.; Fazlollahi, F.; Nikoo, M. K.; Sefidkon, F.; Klemeš, J. J.; Baxter, L. L. Mechanisms and kinetics of CO2 hydrogenation to value added products: A detailed review on current status and future trends. *Renewable Sustainable Energy Rev.* **2017**, *80*, 1292−1311.
(22) Nie, X.; Wang, H.; Janik, M. J.; Guo, X.; Song, C. Computational Investigation of Fe−Cu Bimetallic Catalysts for CO2 Hydrogenation. *J. Phys. Chem. C* **2016**, *120*, 9364−9373.
(23) Nie, X.; Wang, H.; Janik, M. J.; Chen, Y.; Guo, X.; Song, C. Mechanistic Insight into C−C Coupling over Fe−Cu Bimetallic Catalysts in CO2 Hydrogenation. *J. Phys. Chem. C* **2017**, *121*, 13164−13174.
(24) Hwang, S. M.; Han, S. J.; Min, J. E.; Park, H. G.; Jun, K. W.; Kim, S. K. Mechanistic insights into Cu and K promoted Fe catalyzed production of liquid hydrocarbons via CO2 hydrogenation. *J. CO2 Util.* **2019**, *34*, 522−532.
(25) Han, S. J.; Hwang, S. M.; Park, H. G.; Zhang, C.; Jun, K. W.; Kim, S. K. Identification of active sites for CO2 hydrogenation in Fe catalysts by first principles microkinetic modelling. *J. Mater. Chem. A* **2020**, *8*, 13014−13023.
(26) Choi, P. H.; Jun, K. W.; Lee, S. J.; Choi, M. J.; Lee, K. W. Hydrogenation of carbon dioxide over alumina supported Fe K catalysts. *Catal. Lett.* **1996**, *40*, 115−118.
(27) Satthawong, R.; Koizumi, N.; Song, C.; Prasassarakich, P. Bimetallic Fe−Co catalysts for CO2 hydrogenation to higher hydrocarbons. *J. CO2 Util.* **2013**, *3*−*4*, 102−106.
(28) Landau, M. V.; Meiri, N.; Utsis, N.; Vidruk Nehemya, R.; Herskowitz, M. Conversion of CO2, CO, and H2 in CO2 Hydrogenation to Fungible Liquid Fuels on Fe Based Catalysts. *Ind. Eng. Chem. Res.* **2017**, *56*, 13334−13355.
(29) Mears, D. E. Tests for Transport Limitations in Experimental Catalytic Reactors. *Ind. Eng. Chem. Process Des. Dev.* **1971**, *10*, 541−547.
(30) Weisz, P. B.; Prater, C. D. In *Advances in Catalysis and Related Subjects*; Frankenburg, W., Komarewsky, V., Rideal, E., Eds.; Advances in Catalysis, Vol. *6*; Academic Press: New York, NY, 1954; pp 143−196.
(31) Gurvich, L. V.; Iorish, V. S.; Yungman, V. S.; Dorofeeva, O. V. In *CRC handbook of chemistry and physics*; Haynes, W. M., Lide, D. R., Bruno, T. J., Eds.; CRC Press: Boca Raton, FL, 2013; pp 543−565.
(32) Bates, D. M.; Watts, D. G. *Nonlinear regression analysis and its applications*; Wiley: New York, NY, 1988.
(33) Claeys, M.; van Steen, E. In *Fischer−Tropsch Technology*; Steynberg, A., Dry, M., Eds.; Studies in Surface Science and Catalysis, Vol. *152*; Elsevier: Amsterdam, 2004; pp 601−680.
(34) Hwang, J. S.; Jun, K. W.; Lee, K. W. Deactivation and regeneration of Fe K/alumina catalyst in CO2 hydrogenation. *Appl. Catal., A* **2001**, *208*, 217−222.
(35) Kim, J. S.; Lee, S.; Lee, S. B.; Choi, M. J.; Lee, K. W. Performance of catalytic reactors for the hydrogenation of CO2 to hydrocarbons. *Catal. Today* **2006**, *115*, 228−234.
(36) Rodemerck, U.; Holeňa, M.; Wagner, E.; Smejkal, Q.; Barkschat, A.; Baerns, M. Catalyst Development for CO2 Hydro genation to Fuels. *ChemCatChem.* **2013**, *5*, 1948−1955.
(37) Choi, Y. H.; Jang, Y. J.; Park, H.; Kim, W. Y.; Lee, Y. H.; Choi, S. H.; Lee, J. S. Carbon dioxide Fischer−Tropsch synthesis: A new path to carbon neutral fuels. *Appl. Catal., B* **2017**, *202*, 605−610.
(38) Dry, M. E. In *Fischer−Tropsch Technology*; Steynberg, A., Dry, M., Eds.; Studies in Surface Science and Catalysis, Vol. *152*; Elsevier: Amsterdam, 2004; pp 533−600.
(39) Ratkowsky, D. A. A statistically suitable general formulation for modelling catalytic chemical reactions. *Chem. Eng. Sci.* **1985**, *40*, 1623−1628.
(40) van der Laan, G. P.; Beenackers, A. A. C M. Kinetics and Selectivity of the Fischer−Tropsch Synthesis: A Literature Review. *Catal. Rev. Sci. Eng.* **1999**, *41*, 255−318.
(41) Basha, O. M.; Sehabiague, L.; Abdel Wahab, A.; Morsi, B. I. Fischer−Tropsch Synthesis in Slurry Bubble Column Reactors: Experimental Investigations and Modeling − A Review. *Int. J. Chem. Reactor Eng.* **2015**, *13*, 201−288.
(42) Ojeda, M.; Nabar, R.; Nilekar, A. U.; Ishikawa, A.; Mavrikakis, M.; Iglesia, E. CO activation pathways and the mechanism of Fischer−Tropsch synthesis. *J. Catal.* **2010**, *272*, 287−297.
(43) Wang, W.; Jiang, X.; Wang, X.; Song, C. Fe−Cu Bimetallic Catalysts for Selective CO2 Hydrogenation to Olefin Rich C2+ Hydrocarbons. *Ind. Eng. Chem. Res.* **2018**, *57*, 4535−4542.
(44) Iglesias Gonzalez, M. Gaseous Hydrocarbon Synfuels from H2/CO2 based on Renewable Electricity Kinetics, *Selectivity and Fundamentals of Fixed Bed Reactor Design for Flexible Operation*. Ph.D. thesis, Karlsruhe Institute of Technology, 2015.